

A Study of Geometry in Anisotropic Quantum Hall States by Principal Component Analysis

Na Jiang,¹ Siyao Ke,¹ Hengxi Ji,¹ Hao Wang,² Zi-Xiang Hu,³ and Xin Wan^{1,4}

¹*Zhejiang Institute of Modern Physics, Zhejiang University, Hangzhou 310027, P. R. China*

²*Shenzhen Institute for Quantum Science and Engineering and Department of Physics, Southern University of Science and Technology, Shenzhen 518055, P. R. China*

³*Department of Physics and Center for Quantum materials and device, Chongqing University, Chongqing 401331, P. R. China*

⁴*CAS Center for Excellence in Topological Quantum Computation, University of Chinese Academy of Sciences, Beijing 100190, P. R. China*

(Dated: March 3, 2020)

In the presence of mass anisotropy, anisotropic interaction, or in-plane magnetic field, quantum Hall droplets can exhibit shape deformation and internal geometrical degree of freedom. We characterize the geometry of quantum Hall states by principal component analysis, which is a statistical technique that emphasizes variation in a dataset. We first test the method in an integer quantum Hall droplet with dipole-dipole interaction in disk geometry. In the subsequent application to fractional quantum Hall systems with anisotropic Coulomb interaction in torus geometry, we demonstrate that the principal component analysis can quantify the metric degree of freedom and predict the collapse of a $\nu = 1/3$ state. We also calculate the metric response to interaction anisotropy at filling fractions $\nu = 1/5$ and $2/5$ and show that the response is roughly the same within the same Jain sequence, but can differ at large anisotropy for different sequences.

I. INTRODUCTION

In recent years quantum Hall states with broken rotational symmetry have been explored experimentally in systems with anisotropic band mass or in the presence of in-plane magnetic field.¹⁻⁴ A key theoretical question is how we can describe these states beyond model wave functions, which only characterize the topological property of the states and which have no apparent variational parameter. Haldane⁵ pointed out that the geometrical properties of the wave functions have long been overlooked. The Laughlin wave function, for example, is not necessarily associated with rotational symmetry in Laughlin's original proposal;⁶ in fact, it represents a family of wave functions, each with its distinct geometrical parameter. The wave functions can be constructed explicitly, e.g. via a unimodular transformation, which encodes a global metric tensor to accommodate the intrinsic geometry of the wave functions.⁷ These variational wave functions have been demonstrated numerically to characterize the quantum Hall states with mass or interaction anisotropy, as well as in the presence of an in-plane magnetic field.⁷⁻¹⁴

An alternative avenue is to explore the wave function responses of the geometrical disturbance, which can be quantified by an anisotropic mass or interaction metric. Consider an integer quantum Hall droplet with dipole-dipole interaction.¹⁵ The anisotropic interaction effect can be represented by a single mode that distorts the edge of the droplet; the mode has an edge momentum $\Delta M = 2$ for dipolar interaction.¹⁶ Similar to the Gutzwiller wave function for the electron correlation in an on-site Hubbard model,¹⁷ one can introduce a Jastrow factor to account for the geometrical responses. The resulting wave function is consistent with the unimodular construction up to a center-of-mass mode due to the boundary confinement.¹⁶ More exotic excitations, such as emergent gravitons,¹⁸⁻²¹ occur in the fractional case, in which the shape of the exchange-correlation hole, in addition to the overall droplet shape, responds to the metric change. The emergent FQH graviton can

be excited by a geometric quench,²¹⁻²³ which demonstrates its nontrivial dynamics in time.

On the other hand, large anisotropy in mass or interaction can suppress the fractional quantum Hall state.^{9,14} Take the Laughlin state at $\nu = 1/3$ as an example, which is a condensate of composite fermions formed by attaching two vortices to each electron. Heuristically, we can think of the state as a collection of triple zeros for each electron at the location of other electrons, which is encoded in the Laughlin wave function. In the presence of anisotropy, the unimodular transformation split the zeros along the easy axis. Even though we can continue to deform the Laughlin state geometrically, the topological order is expected to be broken once the split of the triple zeros is comparable to the average distance among electrons. The rough estimate of the critical anisotropy that destroys the Laughlin state has been demonstrated numerically to be valid. A liquid crystal like phase emerges for larger anisotropy, which is characterized by incommensurate peaks in the projected static structure factor.⁹

Motivated by the rapid development in machine learning,²⁴ we revisit the anisotropic quantum Hall systems with different interactions and in different geometries. Quantum Hall systems with anisotropic interaction are strongly correlated systems, whose difficulties, in particular beyond the description of model wave functions, lie in the high dimension of the Hilbert space. We approach with dimension reduction in mind, introducing an unsupervised learning, which does not rely on the existence or knowledge of model wave functions, to explore geometrical information from datasets of many-body wave functions obtained by exact diagonalization. Our study finds that the principal component analysis (PCA) method, which has been applied to many physics problems,²⁵⁻³³ serves this purpose well. The leading principal component describes the topology of a family of wave functions, while the subleading components describe the geometry of the states. In particular, the second principal component allows us to extract geometrical excitations, to quantify the in-

trinsic metric of wave functions, and to locate the collapse of topological order. We find that the PCA study reveals that the geometrical response to anisotropic interaction is roughly unchanged in the same Jain series, but differs in different series.

The rest of the paper is organized as follows. We introduce the models for anisotropic quantum Hall systems and the PCA method in Sec. II. The PCA method is tested on integer quantum Hall states on disk geometry with dipole-dipole interaction in Sec. III. In Sec. IV we apply the method to fractional quantum Hall states on torus geometry with anisotropic Coulomb interaction and compare the geometrical responses for filling factor $\nu = 1/3, 2/5$, and $1/5$. We summarize our results in Sec. V and discuss the connection to related work and the potential generalizations.

II. MODELS AND METHOD

A. Anisotropic Interaction

In this study we explore models with two types of interaction: dipole-dipole interaction¹⁶ and coulomb interaction with an in-plane dielectric tensor.⁹ The first interaction is studied in the context of the integer quantum Hall states while the second of the fractional quantum Hall states.

1. Dipole-dipole interaction

In the Bose-Einstein condensation of ^{52}Cr atom³⁴ or the degenerate quantum gas of $^{40}\text{K}^{87}\text{Rb}^{35}$, the interaction can be described as dipole-dipole interaction with the s -wave scattering vanishing for spin polarized fermions. Consider the spin-polarized fermionic dipoles in a symmetric potential

$$U(r) = \frac{1}{2}m(\omega^2x^2 + \omega^2y^2 + \omega_z^2z^2) \quad (1)$$

with radial trap frequency ω , particle mass m , and axial trap frequency ω_z . The system is rotating rapidly around z axis with an angular frequency $\Omega < \omega$. In the fast-rotation limit, the system can be regarded as quasi-2D.^{15,36-38} The motion in the z direction is frozen in its ground state, so we need to integrate out the corresponding degree of freedom. The wave function of the two-body relative coordinate in this direction is

$$\phi(z) = \exp(-z^2/4q^2)/(2\pi q^2)^{1/4}, \quad (2)$$

where q measures the thickness in z direction in units of $l = \sqrt{\hbar/(2m\omega_z)}$. The effective 2D interaction, in the x - y plane, has the form

$$V_{2D}(\vec{\rho}, \theta) = \int dz V_{dd}(\vec{r}, \theta) |\phi(z)|^2 \quad (3)$$

in units of $d^2/(4\pi\epsilon_0l^3)$, where d is the dipole moment and ϵ_0 is the vacuum permittivity. Here, the polarized interaction is

$$V_{dd}(\vec{r}, \theta) = \frac{r^2 - 3(z \cos \theta + x \sin \theta)^2}{r^5}, \quad (4)$$

where θ is the angle between the dipole moment and the z axis. At $\theta = 0$, all dipole moment are oriented in z direction, and thus the system has rotational symmetry. This symmetry is broken while a nonzero component of dipole moment exists in the $x - y$ plane at $\theta \neq 0$. The geometric effect of the anisotropic quantum Hall state and its phase transition can be studied by varying the parameter θ .¹⁴ For moderate θ , the system remains in the quantum Hall phase without rotational symmetry. A phase transition would be expected for larger θ .

In our PCA study below, we consider the anisotropic IQH regime; in this case, the many-body wave functions for different anisotropy have already be characterized in Ref. [16], which can be directly compared to the PCA results.

2. Anisotropic Coulomb interaction

One can introduce anisotropy into FQH systems with Coulomb interaction through anisotropic dielectric tensor or anisotropic band mass, both of which can be represented by a set of generalized pseudopotentials.¹² In this study we explore the geometrical effect in several FQHE states with anisotropy Coulomb interaction with the form

$$V(\rho, A_c) = \frac{e^2}{4\pi\epsilon_0\sqrt{g^{ab}\rho_a\rho_b}} \quad (5)$$

where g^{ab} is diagonal:

$$g^{ab} = \begin{pmatrix} 1/A_c & 0 \\ 0 & A_c \end{pmatrix} = \begin{pmatrix} e^{-A} & 0 \\ 0 & e^A \end{pmatrix} \quad (6)$$

with $A = \ln A_c$. For strong enough magnetic field, the Hamiltonian can be projected into the LLL. The form of the projected Hamiltonian on the torus with Landau gauge is⁴⁰

$$H = \frac{1}{N_\phi} \sum_q V(\vec{q}) e^{-q^2/2} \sum_{i < j} e^{i\vec{q} \cdot (\vec{R}_i - \vec{R}_j)} \quad (7)$$

where N_ϕ is the total quantum flux through the rectangular unit cell and \vec{R}_i is the guiding center coordinate of the i th electron. The Fourier transform of the anisotropic Coulomb interaction is

$$V(\vec{q}) = 1/\sqrt{q_x^2/A_c + A_c q_y^2}. \quad (8)$$

The momentum components q_x and q_y are integral multiples of $2\pi/L_x$ and $2\pi/L_y$, respectively. For moderate anisotropy, the system remains in the FQH phase, while larger A_c can drive the system into a liquid-crystal-like phase.⁹ We study the geometrical effect due to the interaction anisotropy by the PCA for various filling fractions, including $1/3$ and $2/5$ in the first Jain sequence and $1/5$ in the second Jain sequence.³⁹

B. Principal Component Analysis

Quantum Hall systems, as well as other many-body systems, have a huge Hilbert space. In most case, however, we

are only interested in the ground state and a few low-lying excited states. This means that dimension reduction can play an important role in understanding many-particle physics. In this respect, modern machine learning methods play a similar role in extracting limited features from a large dataset of complex systems. These methods explore the fact that even though we have a huge amount of data with considerably many features, the majority of these features that can be used to describe the situation are correlated with each other, leading to much smaller dimensions of interest. Methods of dimension reduction are, therefore, crucial in better understanding the complex systems.

One of the widely used dimension reduction techniques is the PCA.⁴¹ PCA reduces the dimension of samples by linearly projecting them onto a new feature space of fewer dimensions. These new features are called the principal components, which are the main directions along which samples distribute. By using principal components to describe the samples, one can find out their characteristics efficiently.

In this study, we consider a family of normalized real wave functions with a parameter that describes the guiding center geometry of the states. Suppose the wave functions are represented by

$$|\psi^{(\alpha)}\rangle = \sum_{i=1}^D c_i^{(\alpha)} |i\rangle, \quad (9)$$

where $|i\rangle$ represents the many-particle basis with dimension D , while α labels the set of M ground state wave functions with different anisotropy parameter. The PCA searches for a projection matrix P with dimension $d \times D$ that best reproduces the wave functions in reduced dimensions; in other words,

$$\sum_{\alpha=1}^M \left\| P^T P |\psi^{(\alpha)}\rangle - |\psi^{(\alpha)}\rangle \right\|^2 \quad (10)$$

is minimized. Technically, we set up a data matrix of the following form

$$X = \begin{pmatrix} c_1^{(1)} & c_2^{(1)} & \cdots & c_D^{(1)} \\ c_1^{(2)} & c_2^{(2)} & \cdots & c_D^{(2)} \\ \vdots & \vdots & \ddots & \vdots \\ c_1^{(M)} & c_2^{(M)} & \cdots & c_D^{(M)} \end{pmatrix}. \quad (11)$$

The projection is carried out toward the subspace spanned by the eigenvectors of the covariance matrix $X^T X$ with the largest d eigenvalues. In practice, the PCA can find these eigenvectors by the singular value decomposition $X = U \Sigma V^T$ of the data matrix X , where U and V are orthogonal matrices and Σ a diagonal matrix. The covariance matrix of X is thus

$$X^T X = V \Sigma^2 V^T. \quad (12)$$

V^T transform the matrix of wave functions X to

$$Y = X V = \begin{pmatrix} y_1^{(1)} & y_2^{(1)} & \cdots & y_D^{(1)} \\ y_1^{(2)} & y_2^{(2)} & \cdots & y_D^{(2)} \\ \vdots & \vdots & \ddots & \vdots \\ y_1^{(M)} & y_2^{(M)} & \cdots & y_D^{(M)} \end{pmatrix}. \quad (13)$$

The projection is performed in the sense that we are only interested in the first d diagonal elements of Σ and the first d columns of y . The resulting matrix element $y_i^{(\alpha)}$ is, therefore, the projected amplitude of the α th wave function along the i th principal axis. We note that the covariance matrix of Y is diagonal

$$Y^T Y = \Sigma^2 \equiv M \text{diag}(\lambda_1, \lambda_2, \cdots, \lambda_D), \quad (14)$$

where λ_i s are known as explained variance ratios and satisfy $\sum_i \lambda_i = 1$. The principal components with large explained variance ratios spanned the subspace that is an approximate representation of the original set of wave functions. Our goal is to use the resulting projected amplitudes in this subspace to quantify the guiding center geometry of the wave functions.

III. IQH STATES ON DISK GEOMETRY

In this section, we apply PCA to study the wave function deformation of the IQH state in disk geometry with dipole-dipole interaction. The goal here is to demonstrate the feasibility and the simplicity of PCA in understanding the geometrical information of a family of wave functions of the same topological character. As discussed earlier, PCA emphasizes variation and brings out dominating features in a dataset. The analysis in this example thus decipher topology from geometry.

For concreteness, we consider the microscopic system with dipole-dipole interaction as discussed in Sec. II A 1. In a strong harmonic trap with $\alpha = 1.0$, the dipolar fermions are confined at its maximum density except at the perimeter of the droplet.¹⁵ For continuously varying polar angle of the dipoles, we obtain a family of IQH wave functions

$$\Psi_\gamma = e^{-\gamma \sum_{i<j} (z_i - z_j)^2} \left[\prod_{i<j} (z_i - z_j) \right] e^{-\sum_i |z_i|^2/4}, \quad (15)$$

where γ is a variational parameter that describes the geometric shape or the deformation of the IQH droplet.¹⁶ Due to the nontrivial interaction, these states are not simply product states. Their wave functions can be described by the product of the isotropic IQH state and a Jastrow factor that arises in the single-mode approximation of a model quadrupolar interparticle interaction $V(i, j) \propto \Re(z_i - z_j)^2$.¹⁶

The variational wave function suggests that the anisotropic IQH ground state can be written as the superposition of the isotropic IQH state and its edge states with angular momentum increment of integral multiples of 2. These edge states are of the form

$$\Phi_2^p = N_p \left[\sum_{i<j} (z_i - z_j)^2 \right]^p \prod_{i<j} (z_i - z_j) e^{-\sum_i |z_i|^2/4}, \quad (16)$$

where p is a positive integer and N_p the normalization factor.¹⁶ The edge states are orthogonal to each other in the Hilbert space and are, thus, expected to be the principal components, up to a unitary transformation.

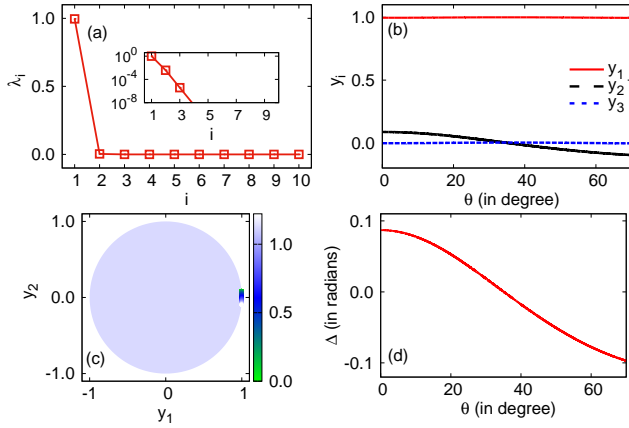


FIG. 1. (Color online) PCA results and analysis for the IQH state with dipole-dipole interaction. (a) The first few explained variance ratios obtained from raw ground state wave functions. The inset displays with log scale. (b) Projections of the various anisotropy strength θ to the three leading principal components. (c) Projection of the samples onto the plane of the two leading principal components. The colorbar indicates the anisotropy strength. (d) The angle Δ between the first projection and the second one as a function of anisotropy strength.

We feed PCA with ground state wave functions for $M = 701$ polar angles θ distributed uniformly between zero and 70° . Fig. 1(a) shows the largest 10 explained variance ratios, among which the first three are sufficiently dominant. This means that even though the interacting IQH states live in a high-dimensional space, their evolution can be well approximated in a rather low-dimensional space. The projected amplitudes y_1 , y_2 , and y_3 along the three principal axes are shown in Fig. 1(b). The deviation of y_3 from zero is already difficult to see by naked eyes, so the evolution is a two-dimensional rotation in the lowest, but an excellent, approximation. We confirm the two-dimensional evolution by plotting y_1 versus y_2 in Fig. 1(c), in which the data falls on the perimeter of the unit circle. The data clusters near x -axis, suggesting that the rotation is limited. By plotting the polar angle Δ (in radians) of the right side of the data in Fig. 1(c) against the polar angle θ (in degrees) of the dipoles in Fig. 1(d), we obtain a geometrical characterization of the ground state wave functions for various θ .

The PCA results of the ground state evolution are expected to be consistent with the wave function decomposition into Φ_2^p [Eq. (16)] based on the physical ground. The quantitative agreement needs an extra rotation because $\Delta_0 \equiv \Delta(\theta = 0) \neq 0$. By minimizing fluctuations, PCA selects the ground state with $\theta = 35^\circ$ to be the first principal component, as evident in Fig. 1(c). After a two-dimensional rotation,

$$\begin{pmatrix} \tilde{y}_1 \\ \tilde{y}_2 \end{pmatrix} = \begin{bmatrix} \cos(\Delta_0) & \sin(\Delta_0) \\ -\sin(\Delta_0) & \cos(\Delta_0) \end{bmatrix} \begin{pmatrix} y_1 \\ y_2 \end{pmatrix}, \quad (17)$$

we expect the first component becomes the isotropic IQH state Φ_0 and the second Φ_2^2 . Fig. 2 compares \tilde{y}_1 and \tilde{y}_2 with the overlaps of wave functions with Φ_0 and Φ_2^2 , respectively,

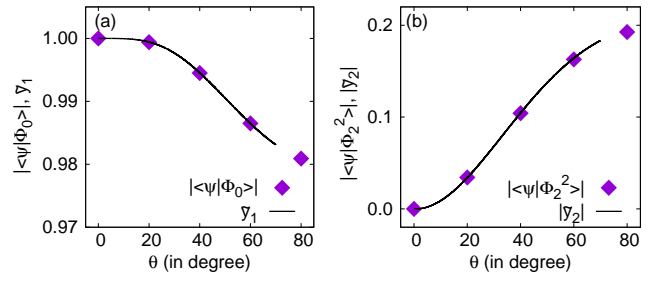


FIG. 2. (Color online) Comparison between rotated projected amplitudes and overlaps of wave functions with Φ_0 and Φ_2^2 in Ref.[9]. (a) The first rotated projected amplitudes \tilde{y}_1 (black solid) is consistent with the overlaps (square) of wave functions with Φ_0 . (b) The absolute value of second rotated projected amplitudes \tilde{y}_2 (black solid) consist with the overlaps (square) of wave functions with Φ_2^2 .

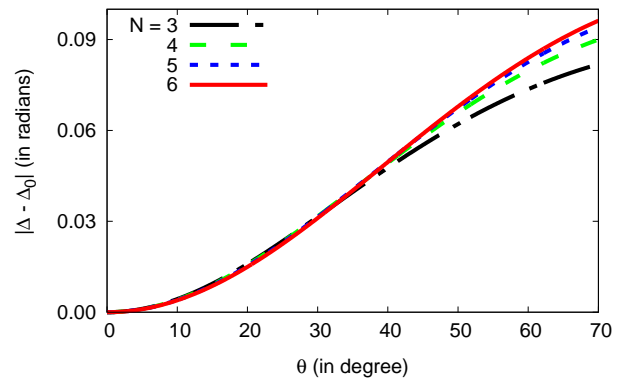


FIG. 3. (Color online) The absolute value of $|\Delta - \Delta_0|$ (in radians) as a function of θ (in degree) for systems with $N = 3 - 6$ particles. For larger systems, the angle curves collapse onto one.

which have been calculated in Ref. [16]. The excellent agreement confirms that PCA, as a well-established tool for dimensional reduction, is effective in separating the geometrical evolution (in subleading principal components) from topology (in the leading component).

For small geometrical distortion, \tilde{y}_2 can be obtained by $\Delta - \Delta_0$ without carrying out the explicit rotation in the reduced space. Therefore, the quantitative comparison suggests that we can identify y_2 , the projection of the ground state on the subleading principal component, with γ , the metric parameter in the variational wave function [Eq. (15)], up to a rotation. Fig. 3 plots $|\Delta - \Delta_0|$ as a function of θ for systems with $N = 3-6$ particles. The system size dependence is found to be negligible for $\theta < 40^\circ$, where the geometrical distortion is sufficiently small so higher-order contributions (beyond two leading principal components) can be omitted.

IV. FQH STATES ON TORUS GEOMETRY

The application of PCA to the anisotropic IQH system is a vivid demonstration of the statistical learning method. The necessity of the method in disk geometry is debatable, as there

exist versatile approaches, such as the Jack polynomial diagonalization⁴² and the Monte Carlo algorithm,⁴³ to relate the wave functions in the first and the second quantization forms. In torus geometry, however, we have less tools. It is, therefore, an interesting problem to explore the applicability of the PCA in closed, translationally invariant systems, especially for the cases that the ground states are not in the form of model wave functions that are exact solutions of corresponding model Hamiltonians.

For this purpose, we turn to the model with anisotropic Coulomb interaction as introduced in Sec. II A 2. In the torus geometry, the ground state wave functions, hence the data matrices, are complex. The transpose in Eqs. (12) and (14), therefore, needs to be replaced by conjugate transpose. The projected amplitude $y_i = y_i^r + iy_i^i$ is now complex.

Earlier study for $\nu = 1/3$ filling⁹ has showed that the Laughlin state remains to be stable but anisotropic for weak interaction anisotropy. For sufficiently strong anisotropy, the system undergoes a transition from the FQH liquid to a liquid-crystal-like state.⁹ Therefore, the motivation of using the PCA here are two-fold. First, for a large range of anisotropy, can the PCA identify the phase transition between the competing ground states? Second, in the Laughlin phase, can the PCA quantify the guiding center metric of the FQH wave functions?

We focus on three families with $\nu = 1/3, 2/5$, and $1/5$ in the following. The first two families belong to the same Jain sequence, in which two flux quanta are attached to each electron in the composite fermion construction. The third, however, combines four flux quanta to each electron in the flux attachment, hence can have more complex geometrical responses.

A. $\nu = 1/3$

We consider electrons with anisotropic Coulomb interaction at $\nu = 1/3$ and feed PCA with ground state wave functions for $N = 10$ electrons with different interaction anisotropy from $A_c = 1.0$ to 1.5 . Fig. 4(a) shows the largest 10 explained variance ratios on both linear and exponential scales. Compared with the integer case, the second ratio becomes visibly nonzero on the linear scale, suggesting that the effect of anisotropy is stronger in this range of A_c in the fractional case. Fig. 4(b) shows the real and imaginary part of the projected amplitudes for the first three components. Even though the wave functions are complex, to a good approximation the imaginary part of the projected amplitudes can be neglected, which means that the geometrical effect of the Laughlin state can be roughly described by a real representation. Compared to the two leading components, $y_3 = y_3^r + iy_3^i$ and other higher-order terms can still be neglected. As shown in Fig. 4(c), the pair (y_1^r, y_2^r) of the data falls on the perimeter of the unit circle. This, again, allows us to calibrate the geometry of the wave function by the shifted polar angle $|\Delta - \Delta_0|$ in Fig. 4(d).

Next, we analyze 106 different ground state wave functions for $A_c = 1.0 - 3.0$. The second largest explained variance

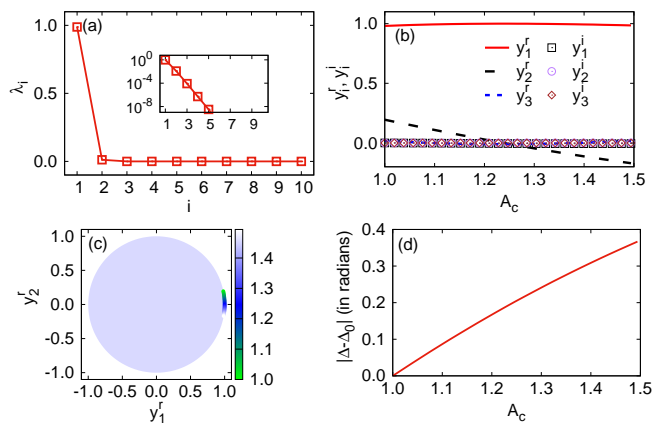


FIG. 4. (Color online) PCA results for anisotropic Coulomb interaction at $\nu = 1/3$ for $N = 10$ electrons with anisotropy strength from 1.0 to 1.5. (a) The largest 10 explained variance ratios on linear scale and insert exponential scale. (b) The real and imaginary part of the projected amplitudes $y_1^{r(i)}, y_2^{r(i)}, y_3^{r(i)}$ for the first three components. (c) The projections of the samples onto the plane of y_1^r and y_2^r . The colorbar indicates the anisotropy strength A_c . (d) The absolute value of the shifted polar angle $|\Delta - \Delta_0|$ (in radians) as a function of anisotropy strength A_c .

ratio is now visibly nonzero, as shown in Fig. 5(a). Fig. 5(b) shows that the imaginary part of the projected amplitudes is still negligible, compared with the corresponding real part. The isotropic ground state has projected components 0.85, 0.51, and 0.15 along the three leading principal directions. We can neglect y_3 again, which contributes no more than 2.3% to the ground states, and plot $|y_1|$ versus $\text{sgn}(y_2^r)|y_2|$ in Fig. 5(c). To a good approximation, the data falls on the perimeter of the unit circle, indicating that the evolution can be described by the relative weight change of two wave functions. After a rotation in the $|y_1| - \text{sgn}(y_2^r)|y_2|$ plane, as defined in Eq. (17), we plot \tilde{y}_1 and \tilde{y}_2 as functions of A_c in Fig. 5(d). As discussed in the IQH case, \tilde{y}_1 is the projection of the ground state wave functions on the isotropic one at $A_c = 1$. The projection \tilde{y}_2 on the other axis exceeds \tilde{y}_1 at $A_c = 2.2$, indicating a phase transition from the Laughlin phase to a different phase induced by strong anisotropic interaction. This value is in good agreement with $A_c \approx 2.0$ identified by the sudden collapse of the excitation energy gap. In practice, the rotation is not necessary, because the transition point can be determined by $|\Delta_c - \Delta_0| = \pi/4$.

B. $\nu = 2/5$

The FQH effect at $\nu = 1/3$ can be regarded as the $\nu = 1$ IQH effect of composite fermions, in which two magnetic flux quanta are attached to each electron. We now turn to an $N = 10$ electron system at $\nu = 2/5$ in the same Jain sequence with two composite fermion LLs filled. We apply PCA to 32 ground state wave functions from anisotropic Coulomb interaction with $A_c = 1.0 - 1.5$. Fig. 6 shows the 10 lead-

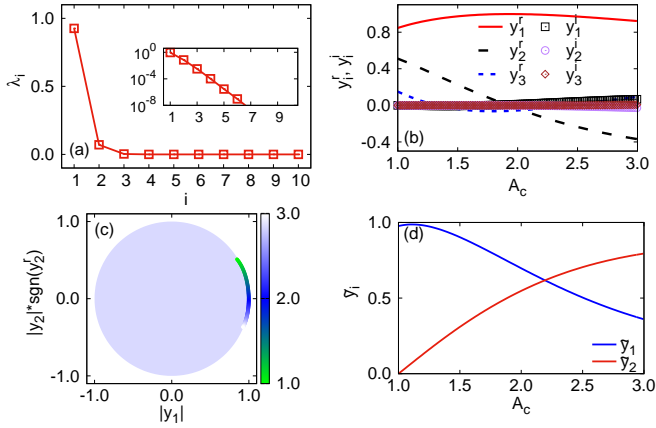


FIG. 5. (Color online) PCA results for anisotropic Coulomb interaction at $\nu = 1/3$ for $N = 10$ electrons with anisotropy strength from 1.0 to 3.0. (a) The largest 10 explained variance ratios on linear scale and insert exponential scale. (b) The real and imaginary part of the projected amplitudes $y_1^{r(i)}$, $y_2^{r(i)}$, $y_3^{r(i)}$ for the first three components. (c) The projections of the samples onto the plane of $|y_1|$ and $\text{sgn}(y_2^r)|y_2|$. The colorbar indicates the anisotropy strength A_c . (d) The rotated projected amplitudes \tilde{y}_1 and \tilde{y}_2 as functions of anisotropy strength A_c .

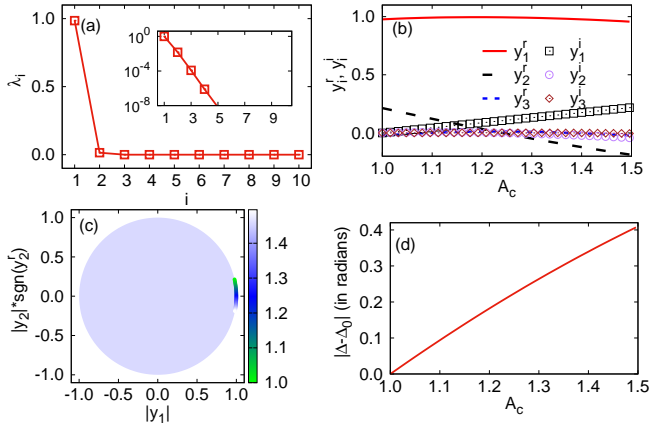


FIG. 6. (Color online) PCA results for anisotropic Coulomb interaction at $\nu = 2/5$ for $N = 10$ electrons with anisotropy strength from 1.0 to 1.5. (a) The largest 10 explained variance ratios on linear scale and insert exponential scale. (b) The real and imaginary part of the projected amplitudes $y_1^{r(i)}$, $y_2^{r(i)}$, $y_3^{r(i)}$ for the first three components. (c) The projections of the samples onto the plane of $|y_1|$ and $\text{sgn}(y_2^r)|y_2|$. The colorbar indicates the anisotropy strength A_c . (d) The absolute value of the shifted polar angle $|\Delta - \Delta_0|$ (in radians) as a function of anisotropy strength A_c .

ing explained variance ratios, the amplitudes projected to the first three axes, the evolution of $(|y_1|, \text{sgn}(y_2^r)|y_2|)$, and the variation of $|\Delta - \Delta_0|$ as a function of A_c . The results are very similar to those in Fig. 4, implying that the additional composite fermion LL does not affect the metric of the wave functions. We note that the imaginary part of y_i can, again, be neglected.

To quantitatively compare the geometrical effect for $\nu =$

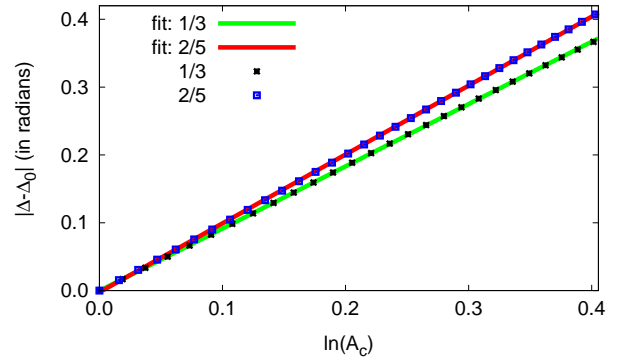


FIG. 7. (Color online) Comparison of $|\Delta - \Delta_0|$ between $\nu = 1/3$ and $2/5$ states. The data can be fitted by a straight line $0.92 \ln A_c$ for $1/3$ case and $1.02 \ln A_c$ for $2/5$ state.

$1/3$ and $2/5$, we plot $|\Delta - \Delta_0|$ as a function of $A = \ln A_c$ for the two cases in Fig. 7. Data in each case can be fitted by a straight line

$$|\Delta - \Delta_0| = c \ln A_c \quad (18)$$

where the slope $c = 0.92$ for $\nu = 1/3$ and $c = 1.02$ for $\nu = 2/5$. The linear dependence in Eq. (18) can be understood as the linear response of the wave function metric to the interaction metric, as there is only one parameter in the wave functions, which also characterizes the split of the two flux quanta from each electron in the composite fermion picture. The 10% difference in the prefactor of the linear term is likely due to the fact that each composite fermions LL at $\nu = 2/5$ has too few particles, because noticeable deviations also show in the IQH case for $N = 3$ and 4 electrons in Fig. 3.

C. $\nu = 1/5$

The similarities between $\nu = 1/3$ and $2/5$ motivate us to explore the comparison between $\nu = 1/3$ and $1/5$. The latter two correspond to the filling of $\nu = 1$ composite fermion LL. However, for $\nu = 1/5$, there are four flux quanta attached to each electron. In the presence of geometrical distortion, it is not obvious why the four flux quanta should split in proportion, hence nonlinear dependence in $\ln A_c$ can go beyond Eq. (18). We consider 8 electrons at $1/5$ filling with anisotropic Coulomb interaction for $A_c = 1.0 - 1.5$ in torus geometry. The PCA results for 32 ground state wave functions are summarized in Fig. 8. Unlike in Fig. 4(b), we find that the projected amplitudes now have significant imaginary parts. However, the magnitudes of the first two components still dominate and, again, fall roughly on the perimeter of the unit circle. Nevertheless, the resulting variation of $|\Delta - \Delta_0|$ bends up as a function of A_c in Fig. 8(d), as oppose to the bending down in Fig. 4(d). This indicates that the geometrical effect is stronger in the $1/5$ case.

For further comparison, we plot $|\Delta - \Delta_0|$ as a function of $A = \ln A_c$ in Fig. 9 for both $\nu = 1/3$ and $1/5$. We choose the

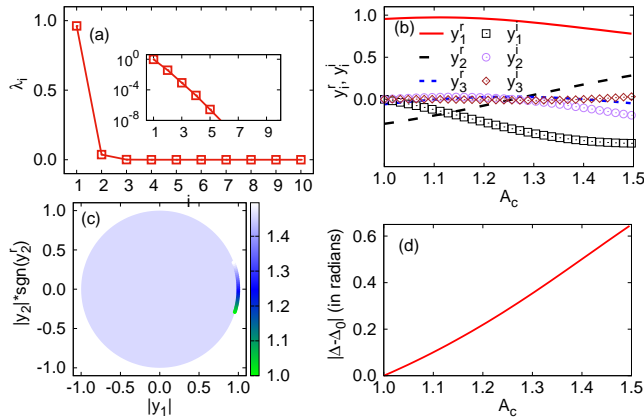


FIG. 8. (Color online) PCA results for anisotropic Coulomb interaction at $\nu = 1/5$ for $N = 8$ electrons with anisotropy strength from 1.0 to 1.5. (a) The largest 10 explained variance ratios on linear scale and insert exponential scale. (b) The real and imaginary part of the projected amplitudes $y_1^{r(i)}$, $y_2^{r(i)}$, $y_3^{r(i)}$ for the first three components. (c) The projections of the samples onto the plane of $|y_1|$ and $\text{sgn}(y_2^r)|y_2|$. The colorbar indicates the anisotropy strength A_c . (d) The absolute value of the shifted polar angle $|\Delta - \Delta_0|$ (in radians) as a function of anisotropy strength A_c .

same range of A_c from 1.0 to 1.4 to compare and note that the dependence on the range is negligible, as long as we do not approach the critical A_c for the collapse of the FQH states. In particular, strong anisotropy also destroy the 1/5 state, but the critical A_c is estimated by PCA to be 1.62. For $\nu = 1/3$, we find

$$|\Delta - \Delta_0|_{\nu=1/3} = 0.92 \ln A_c, \quad (19)$$

as discussed above. For $\nu = 1/5$, on the other hand, the curve can be fitted by

$$|\Delta - \Delta_0|_{\nu=1/5} = 0.95 \ln A_c + 1.64(\ln A_c)^2. \quad (20)$$

Interestingly, the linear responses are roughly equal in the two cases, which is also not far from 1.02 for $\nu = 2/5$, while the 1/5 case has an additional quadratic contribution that cannot be neglected.

V. SUMMARY AND DISCUSSION

In this paper, we propose to use PCA, a popular statistical learning method, to study the geometrical responses of the quantum Hall wave functions to anisotropic interaction. We demonstrated that for moderate anisotropy, the emphasis on variation by PCA allows a natural separation of topology and geometry. The analysis quantifies the geometrical effect in the projection to the axis corresponding to second largest explained variance ratio, while the leading one encodes the topological wave function, up to a trivial rotation.

The method can also quantitatively identify the transition from the topological phase to the CDW phase induced by

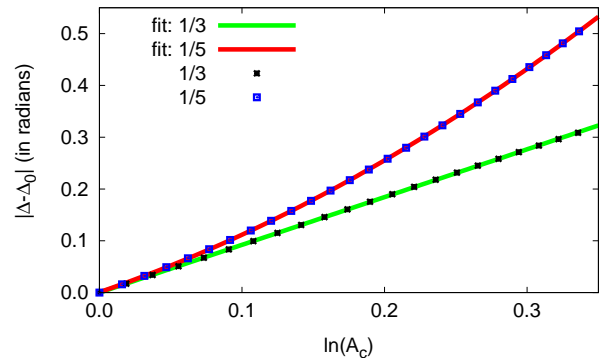


FIG. 9. (Color online) Comparison of $|\Delta - \Delta_0|$ between $\nu = 1/3$ and $1/5$ states. The data can be fitted by $0.92 \ln A_c$ for 1/3 case and $0.95 \ln A_c + 1.64(\ln A_c)^2$ for 1/5 state.

anisotropy. Interestingly, PCA reveals that the wave function evolution with increasing anisotropic Coulomb interaction can be approximated by a linear interpolation of two wave functions, one representing the topological phase and the other the CDW phase. This approximation is satisfactory all the way across the anisotropy induced quantum phase transition.

For FQH states in the primary Jain sequence, in which each composite fermion contains two magnetic flux quanta, PCA finds that the geometrical responses are linear in $(\ln A_c)$, which is the logarithm of the diagonal element in the anisotropic interaction metric. The amplitude of the responses are comparable for $\nu = 1/3$ and $2/5$, which have one and two filled composite fermion LLs, respectively.

On the other hand, for a different Jain sequence in which each composite fermion has four magnetic flux quanta, PCA reveals a strong nonlinear geometrical responses. The geometrical effect for $\nu = 1/5$, quantified by the projection to the subleading axis, is dominantly quadratic in $(\ln A_c)$, even though it has a linear contribution of a similar amplitude as in the 1/3 case. The surprising result suggests that the four flux quanta in each composite fermions are not split in simple linear fashion. Further wave function analysis of the $\nu = 1/5$ case in disk or sphere geometry is needed for a clearer picture.

In a very recent paper, Ippoliti *et al.*⁴⁴ studied the geometry of flux attachment in anisotropic FQH states with anisotropic mass and isotropic Coulomb interaction, which is equivalent to isotropic mass with anisotropic interaction after introducing anisotropic LL orbitals. The authors used an infinite density matrix renormalization group (iDMRG) algorithm to study the response of the internal wave function metric to band mass anisotropy, which was extracted from guiding center structure factor. They found that the geometrical response is approximately the same for states in the same Jain sequence, but differs substantially between different sequences. For $\nu = 1/3$, we draw a similar conclusion that the geometrical response is dominated by a linear term, which corresponds to the internal unimodular metric. However, for $\nu = 1/5$, while the iDMRG study found significant difference in the prefactor of the linear response from that of $\nu = 1/3$, we find a similar linear response but very different quadratic response. We note

that the iDMRG study also found larger quadratic responses in isotropic rescaling, but the results showed strong size dependence.

The main advantage of the PCA in this study, compared to more conventional method,⁷ is that one can quantify geometrical degree of freedom without the explicit knowledge of model wave functions. We thus expect the approach can be easily generalized to more complex filling fractions, where explicit wave functions cannot be given analytically, or are difficult to represent numerically. In addition, systems with disorder can also be treated with this technique.

VI. ACKNOWLEDGEMENTS

The work at Zhejiang University was supported by the National Natural Science Foundation of China through Grant No.

11674282, the Strategic Priority Research Program of Chinese Academy of Sciences Grant No. XDB28000000, and the National Basic Research Program of China through Project No. 2015CB921101. HW is supported by the National Natural Science Foundation of China Grant No. 11474144. ZXH is supported by the National Natural Science Foundation of China Grants No. 11674041 and No. 11974064.

-
- ¹ J. Xia, J. P. Eisenstein, L. N. Pfeiffer, and K. W. West, *Nat. Phys.* **7**, 845 (2011).
- ² D. Kamburov, Y. Liu, M. Shayegan, L.N. Pfeiffer, K.W. West, and K.W. Baldwin, *Phys. Rev. Lett.* **110**, 206801 (2013).
- ³ M. P. Lilly, K. B. Cooper, J. P. Eisenstein, L. N. Pfeiffer, and K. W. West, *Phys. Rev. Lett.* **82**, 394 (1999).
- ⁴ I. Jo, K. A. V. Rosales, M. A. Mueed, L. N. Pfeiffer, K.W. West, K.W. Baldwin, R.Winkler, M. Padmanabhan, and M. Shayegan, *Phys. Rev. Lett.* **119**, 016402 (2017).
- ⁵ F. D. M. Haldane, *Phys. Rev. Lett.* **107**, 116801 (2011).
- ⁶ R. B. Laughlin, *Phys. Rev. Lett.* **50**, 1395 (1983).
- ⁷ R.-Z. Qiu, F. D. M. Haldane, X. Wan, K. Yang, and S. Yi, *Phys. Rev. B* **85**, 115308 (2012).
- ⁸ B. Yang, Z. Papić, E. H. Rezayi, R. N. Bhatt, and F. D. M. Haldane, *Phys. Rev. B* **85**, 165318 (2012).
- ⁹ H. Wang, R. Narayanan, X. Wan, and F. C. Zhang, *Phys. Rev. B* **86**, 035122 (2012).
- ¹⁰ V. M. Apalkov and T. Chakraborty, *Solid State Commun.* **177**, 128 (2014).
- ¹¹ Z. Papić, *Phys. Rev. B* **87**, 245315 (2013).
- ¹² B. Yang, Z.-X. Hu, C. H. Lee, and Z. Papić, *Phys. Rev. Lett.* **118**, 146403 (2017).
- ¹³ L.-P. Yang, Q. Li, and Z.-X. Hu, *Chin. Phys. B* **27**, 087306 (2018).
- ¹⁴ Z.-X. Hu, Q. Li, L.-P. Yang, W.-Q. Yang, N. Jiang, R.-Z. Qiu, and B. Yang, *Phys. Rev. B* **97**, 035140 (2018).
- ¹⁵ R.-Z. Qiu, S.-P. Kou, Z.-X. Hu, X. Wan, and S. Yi, *Phys. Rev. A* **83**, 063633 (2011).
- ¹⁶ R.-Z. Qiu, Z.-X. Hu, and X. Wan, *Phys. Rev. B* **88**, 235118 (2013).
- ¹⁷ see, e.g., P. Fulde, *Electron Correlations in Molecules and Solids*, 3rd ed. (Springer, Berlin, Heidelberg 1995) p. 100.
- ¹⁸ B. Yang, Z.-X. Hu, Z. Papić, and F. D. M. Haldane, *Phys. Rev. Lett.* **108**, 256807 (2012).
- ¹⁹ K. Yang, *Phys. Rev. B* **93**, 161302 (2016).
- ²⁰ S. Golkar, D. X. Nguyen, and D. T. Son, *JHEP* **01**, 021 (2016).
- ²¹ S-F. Liou, F. D. M. Haldane, K. Yang, and E. H. Rezayi, *Phys. Rev. Lett.* **123**, 146801 (2019).
- ²² Z. Liu, A. Gromov, and Z. Papić, *Phys. Rev. B* **98**, 155140 (2018).
- ²³ M. F. Lapa, A. Gromov, and T. L. Hughes, *Phys. Rev. B* **99**, 075115 (2019).
- ²⁴ I. Goodfellow, Y. Bengio, and A. Courville, *Deep Learning* (MIT Press 2016).
- ²⁵ L. Wang, *Phys. Rev. B* **94**, 195105 (2016).
- ²⁶ J. Carrasquilla and R. Melko, *Nat. Phys.* **13**, 431 (2017).
- ²⁷ G. Carleo, M. Troyer, *Science* **355**, 602 (2017).
- ²⁸ X. Gao and L.-M. Duan, *Nat. Comm.* **8**, 662 (2017).
- ²⁹ C. Wang and H. Zhai, *Phys. Rev. B* **96**, 144432 (2017).
- ³⁰ S. J. Wetzel, *Phys. Rev. E* **96**, 022140 (2017).
- ³¹ W. Hu, R. R. P. Singh, and R. T. Scalettar, *Phys. Rev. E* **95**, 062122 (2017).
- ³² N. C. Costa, W. Hu, Z. J. Bai, R. T. Scalettar, and R. R. P. Singh, *Phys. Rev. B* **96**, 195138 (2017).
- ³³ C. Wang and H. Zhai, *Front. Phys.* **13**, 130507 (2018).
- ³⁴ A. Griesmaier, J. Werner, S. Hensler, J. Stuhler, and T. Pfau, *Phys. Rev. Lett.* **94**, 160401 (2005).
- ³⁵ C. J. Myatt, E. A. Burt, R. W. Ghrist, E. A. Cornell, and C. E. Wieman, *Phys. Rev. Lett.* **78**, 586 (1997).
- ³⁶ N. R. Cooper, *Advances in Physics* **57**, 539 (2008).
- ³⁷ A. L. Fetter, *Rev. Mod. Phys.* **81**, 647 (2009).
- ³⁸ M. A. Baranov, H. Fehrmann, and M. Lewenstein, *Phys. Rev. Lett.* **100**, 200402 (2008).
- ³⁹ J. K. Jain, *Composite Fermions* (Cambridge University Press, New York, 2007).
- ⁴⁰ E. H. Rezayi and F. D. M. Haldane, *Phys. Rev. Lett.* **84**, 4685 (2000).
- ⁴¹ K. Pearson, *Philos. Mag.* **2**, 559 (1901).
- ⁴² K. H. Lee, Z.-X. Hu, and X. Wan, *Phys. Rev. B* **89**, 165124 (2014).
- ⁴³ Y. Zhang, Y.-H. Wu, J. A. Hutasoit, and J. K. Jain, *Phys. Rev. B* **90**, 165104 (2014).
- ⁴⁴ M. Ippoliti, R. N. Bhatt, and F. D. M. Haldane, *Phys. Rev. B* **98**, 085101 (2018).